With this agreement as a sign of convergence, I have used USPs with the 29.1-Ry cutoff to select promising candidate water adsorption structures, and PAWs with the higher cutoff to check and refine the results. This calculation was done only at the experimental ice-Ih volume (D. R. Hamann, private communication). Because energy varies slowly with volume near a minimum, the effect of not optimizing the lattice parameter in the NCPP calculation is no more than a few meV—and in the right direction relative to agreement with the present PAW result.

20. Similar LEED *I-V* curves were reported in (*5*, *6*) for H_2O and D_2O adlayers on Ru(0001), implying similar local geometries for the two molecules. This means that the local geometry was not affected much by the mass of H versus that of D and that ignoring quantum effects is a reasonable approximation, if one is trying to understand a local effect such as the near coplanarity of the adlayer O atoms.
21. To sample the surface brillouin zone (SBZ) for the $\sqrt{3} \times \sqrt{3}$ supercell, I used a 4 × 4 set of equally spaced k vectors, and for the larger cell a 2 × 2 k vector set. In all the adsorption calculations discussed here, I accelerated electronic relaxation using Methfessel and Paxton's Fermi-level smearing method (width = 0.2 eV) (*40*). I corrected for the contact potential difference associated with adsorbing water on only one side of an Ru slab using Kresse's adaptation (*41*) of Neugebauer and Scheffler's method (*42*). Because Held and Menzel's LEED results imply that water prefers bonding in atop sites (i.e., with the O atom directly above an Ru, rather than in a two- or threefold site) (*3*), in agreement with numerous earlier calculations (*8*), I did not consider adlayer geometries in which O atoms bridge Ru atoms or reside in threefold hollows. Similarly, because Held and Menzel report that D_2O/Ru(0001) produces a sharp $\sqrt{3} \times \sqrt{3}$ LEED pattern, I only considered geometries where this would occur.
22. Using a 12-molecule per supercell Bernal-Fowler ice-Ih model, the PW'91 exchange-correlation potential (*1*, *2*), a hard NCPP, and a plane-wave basis cutoff of 130 Ry, Hamann finds a sublimation energy of 0.66 eV. The experimental value, removing zero-point energy to allow direct comparison, is 0.61 eV (*23*, *24*). Hamann reported a theoretical E_{sub} of 0.55 eV in (*38*). The new theoretical value, 0.66 eV, follows the correction of a problem with the variable grid used in that work.
23. E. Whalley, in *The Hydrogen Bond*, P. Schuster, G. Zundel, C. Sandorfy, Eds. (North-Holland, Amsterdam, 1976), vol. 3, pp.1425–1470.
24. According to the analysis in (*23*), zero-point vibration reduces the 0 K sublimation energy of H_2O by 120 meV and of D_2O ice by 98 meV.
25. PAW results are also listed in Table 2 to provide a convergence check. The PAW preference for ice is ~0.17 eV, compared with 0.19 eV for the same structures but with the use of USPs. Thus, lack of basis convergence is not the source of weak binding of undissociated water structures to Ru(0001).
26. This agrees, qualitatively, with the finding (*43*) of an energy cost of several tenths of an electron volt to move an adsorbed H to a subsurface octahedral site.
27. Y. Lilach, L. Romm, T. Livneh, M. Asscher, *J. Phys. Chem. B* **105**, 2736 (2001).
28. G. Pirug, C. Ritke, H. P. Bonzel, *Surf. Sci.* **241**, 289 (1991).
29. R. L. Kurtz, R. Stockbauer, T. E. Madey, E. Roman, J. L. de Segovia, *Surf. Sci.* **218**, 178 (1989).
30. P. A. Thiel, R. A. de Paola, F. M. Hoffmann, *J. Chem. Phys.* **80**, 5326 (1984).
31. P. J. Feibelman, D. R. Hamann, *Surf. Sci.* **179**, 153 (1987).
32. M. A. Barteau, J. Q. Broughton, D. Menzel, *Surf. Sci.* **133**, 443 (1983).
33. M. Nakamura, M. Ito, *Chem. Phys. Lett.* **325**, 293 (2000).
34. As noted in (*4*), they should be attracted back to the surface by image forces.
35. P. Feulner, D. Menzel, unpublished data.
36. ESD of the dissociated H atoms of the half-dissociated structure should also be weak.
37. A mosaic of $\sqrt{3} \times \sqrt{3}$ patches with H-up waters only in their central regions.
38. D. R. Hamann, *Phys. Rev. B* **55**, R10157 (1997).
39. The theoretical sublimation energy equals the energy of a single D_2O molecule less 1/12 the energy of the 12-molecule supercell.
40. M. Methfessel, A. T. Paxton, *Phys. Rev. B* **40**, 3616 (1989).
41. G. Kresse, VASP Guide, http://cms.mpi.univie.ac.at/vasp/guide/node143.html.
42. J. Neugebauer, M. Scheffler, *Phys. Rev. B* **46**, 16067 (1992).
43. M. Y. Chou, J. R. Chelikowski, *Phys. Rev. B* **39**, 5623 (1989).

44. I am grateful to D. R. Jennison for alerting me to the problem of accounting theoretically for Held and Menzel's LEED geometry; N. D. Shinn, B. C. Bunker, D. Menzel, and T. E. Madey for helpful discussions; and D. R. Hamann, D. M. Teter, and G. Kresse for assistance in establishing a baseline for the accuracy of H bonding calculations. VASP was developed at the Institut für Theoretische Physik of the Technische Universität Wien. Supported, in part, by the DOE Office of Basic Energy Sciences, Division of Material Sciences. Sandia is a multiprogram laboratory operated by Sandia Corporation, a Lockheed Martin Company, for the United States DOE under contract DE-AC04-94AL85000.

17 August 2001; accepted 6 November 2001

Electrically Driven Single-Photon Source

Zhiliang Yuan,[1] Beata E. Kardynal,[1] R. Mark Stevenson,[1] Andrew J. Shields,[1]* Charlene J. Lobo,[2] Ken Cooper,[2] Neil S. Beattie,[1,2] David A. Ritchie,[2] Michael Pepper[1,2]

Electroluminescence from a single quantum dot within the intrinsic region of a p-i-n junction is shown to act as an electrically driven single-photon source. At low injection currents, the dot electroluminescence spectrum reveals a single sharp line due to exciton recombination, while another line due to the biexciton emerges at higher currents. The second-order correlation function of the diode displays anti-bunching under a continuous drive current. Single-photon emission is stimulated by subnanosecond voltage pulses. These results suggest that semiconductor technology can be used to mass-produce a single-photon source for applications in quantum information technology.

The emerging field of quantum information technology requires the development of a new type of light source, in which the photon number can be carefully controlled. Especially useful is an emitter of single photons at predetermined times. However, it is impossible to generate single photons with even very faint laser pulses, for which the photon number obeys Poissonian statistics. It has been shown that the unavoidable multiphoton pulses produced by a laser render quantum cryptography insecure from certain types of eavesdropping attack (*1*). Thus, unconditionally secure quantum cryptography, in addition to other applications in photonic quantum computing (*2*) and communications, requires the development of a true single-photon source. The generation of light with sub-Poissonian fluctuations in the photon number is also useful for performing optical measurements at lower noise levels than is possible with classical light. We report here the realization of an electrically driven source of single photons based on integrating quantum dots into a conventional semiconductor light-emitting diode structure.

Single photons can be generated through laser excitation and subsequent fluorescence of a single quantized system, such as an atom or an ion (*3*). Recently, this concept has been extended to several other quantum systems, such as single dye molecules (*4–8*), single quantum dots (*9–13*), and single nitrogen vacancy centers in diamond (*14*, *15*). In each of these experiments or proposals, the emission was stimulated by optical excitation with an incident laser. However, from the viewpoint of practical application, one would prefer an electrically driven photon source. Early proposals for constructing an electrical single-photon source suggested using the Coulomb blockade effect to inject single electrons and holes into an etched double-barrier mesoscopic heterojunction (*16*). However, experimental studies on such a structure required operation at milli-kelvin temperatures, whereas the collected photon rate was too weak to allow the second-order correlation function to be verified (*17*). It was also theoretically proposed that a single quantum dot could be used, not just for emission of single photons but also for generation of entangled pairs of photons (*18*). Another proposal was based on injecting single electrons, confined within the moving potential wells defined by a surface acoustic wave and a split gate, into a p-type region (*19*).

We study the photo- and electroluminescence of a p-i-n diode containing a layer of InAs self-organized quantum dots in the in-

[1]Toshiba Research Europe Limited, Cambridge Research Laboratory, 260 Cambridge Science Park, Milton Road, Cambridge, CB4 0WE, UK. [2]Cavendish Laboratory, University of Cambridge, Madingley Road, Cambridge, CB3 0HE, UK.

*To whom correspondence should be addressed: E-mail: andrew.shields@crl.toshiba.co.uk

trinsic region. In order to avoid the nonradiative recombination associated with etched surfaces, relatively large mesas were prepared containing many quantum dots and their surface apertured, so as to collect the emission from just one dot. The electroluminescence spectra of the diode display sharp lines due to excitonic transitions in individual dots, which, as verified by photon pair correlation measurements, generate sequential emission of individual photons.

In our device structure (Fig. 1A), the semiconductor layers were grown by molecular beam epitaxy on a GaAs substrate and consist of a GaAs p-i-n diode with a layer of nominally nanometer-scale InAs self-organized quantum dots (*20*) inserted into the intrinsic region. Atomic force microscopy of dot layers grown under similar conditions (Fig. 1C) reveals that the dots have an areal density of $\sim 5 \times 10^8$ cm^{-2}. The structure was etched into mesas with lateral dimensions of 10×10 μm and ohmic contacts were formed to the n- and p-type regions (Fig. 1B). The emissive area was defined by means of an aperture in the opaque metal layers on the device surface. The p-i-n diodes were found to display nearly ideal current-voltage (*I-V*) characteristics, with the injected current increasingly rapidly around a forward bias of 1.5 V (Fig. 2C).

Electroluminescence spectra recorded on the diode at 5 K with different biases applied between the n- and p-type contacts (Fig. 2A) show that at low injection currents, a sharp line is observed near 1.3942 eV, the intensity of which increases approximately linearly with I (Fig. 2B); a best fit to the data shows that the intensity strengthens as $I^{1.1}$. Based on this current dependence, we ascribe this line to recombination of the single exciton (X) of one electron and one hole within a quantum dot. At higher injection currents, the X line weakens and a second strong line (marked X_2) appears at 4.7 meV higher energy. This line, which strengthens with current as $I^{2.0}$, is ascribed to the biexciton transition of the dot. The strength of X drops for currents in excess of 5 μA because of competition from the biexciton state. On the other hand, the biexciton intensity is seen to saturate at the highest currents, which suggests that tri- and higher order excitons cannot be excited in these dots. This is presumably because, due to the small size of the dots studied here, they have only one electron- or hole-confined level. The maximum intensity of the biexciton line is stronger than that of the exciton, because of its shorter lifetime and the fact that at high injection currents, the average occupancy of the biexciton state can approach unity, whereas at the intermediate currents for which X dominates, there is always a statistical distribution in the occupancy of the empty, exciton, and biexciton states.

The same transitions, with similar photon energy and linewidth, can also be observed in the photoluminescence spectra recorded on the structure (*21*). The X line showed an approximately linear dependence on laser power, whereas a quadratic increase was seen for X_2, lending further credence to our assignment of the two peaks. Time-resolved photoluminescence measurements on the same dot determined the exciton and biexciton lifetimes to be 1.02 and 0.47 ns, respectively. We also observe the X decay to be delayed relative to X_2 at high laser power, as one would expect, because the biexciton photon is emitted before the exciton (*13*). Similar characteristics are seen in the time-resolved electroluminescence.

We measured the photon pair correlation statistics of the electroluminescence using a Hanbury-Brown and Twiss arrangement (Fig. 3D) of a 50/50 beamsplitter and two Silicon photon-counting avalanche photodiodes (*22*). A time-correlated single-photon counting card was used to repeatedly measure the time delays, τ, between photons registered by the two detectors, from which a histogram of the

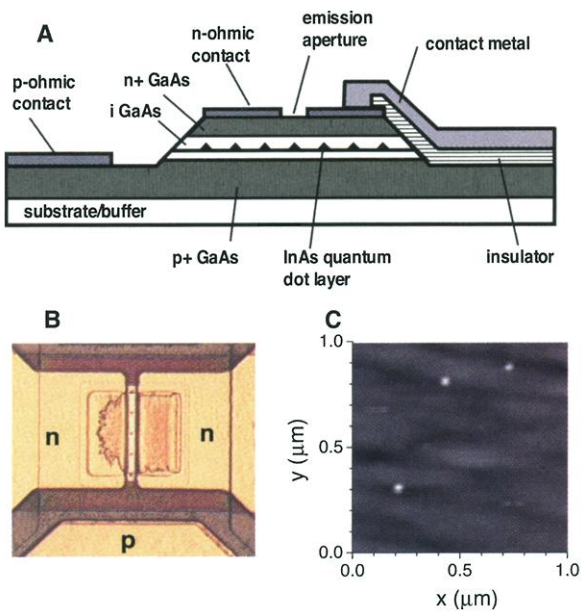

Fig. 1. (**A**) Schematic of the single-photon–emitting diode in cross section. (**B**) Image of the device in an optical microscope. (**C**) Atomic force micrograph of a quantum dot layer grown under similar conditions to those in the device.

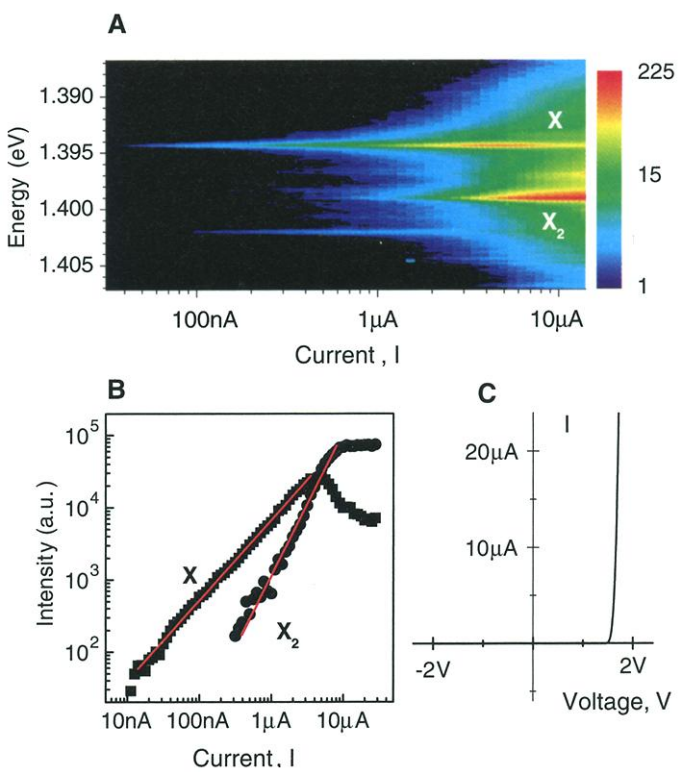

Fig. 2. The electroluminescence spectra of the single-photon–emitting diode, showing sharp line emission characteristic of individual quantum dots. (**A**) Electroluminescence intensity from the device as a function of emission photon energy (vertical axis) and drive current (horizontal axis). Sharp line emission (marked X and X_2) is seen arising from a single quantum dot in the structure. (**B**) Measured (symbols) dependence of the intensities of the X and X_2 lines on the injection current. The solid lines show a linear fit to the low-current data. (**C**) *I-V* characteristic of the device shows ideal diode-like behavior.

number of occurrences of different time delays was compiled. This histogram is proportional to the second-order correlation function $g^{(2)}(\tau)$ in the low count rate limit, where the average time between detected photons is much longer than the measured delays τ. For an ideal single-photon emitter, we would expect to find no occurrences of zero time delay; that is, two photons should never be emitted simultaneously.

Figure 3A (i through iii) plots the correlation signal recorded for the single exciton electroluminescence with different injection currents. The dip in the correlation signal $g^{(2)}(\tau)$ at zero time delay, $\tau = 0$, which is the signature of a single-photon source, is clearly observed. This demonstrates the strong suppression of two photon emission events from the quantum dot, which occurs because, after photon emission, there is a finite delay before the dot is repopulated and can re-emit. In contrast, emission from the two-dimensional wetting layer on which the dots form [Fig. 3A (v)] displays a flat correlation trace, as expected for Poissonian statistics.

The dip in $g^{(2)}(\tau)$ does not fall completely to zero. For the lowest injection current of 2 μA, we find $g^{(2)}(0) = 0.34$ [Fig. 3A (i)]. However, this is largely due to the finite time resolution of the measurement system, which was measured to be 0.85 ns (full width at half maximum) rather than two photon emission events from the dot. We calculated $g^{(2)}(\tau)$ using a simple rate equation model to describe the occupancies of the biexciton, exciton, and empty states of the dot at different injection current densities (Fig. 3B, thin lines). The simulation also takes account of the dark counts of the single-photon detectors, as well as background electroluminescence, which add a flat contribution to $g^{(2)}(\tau)$ that is always less than 0.14. The correlation dip sharpens as the current increases, due to an increase in the electron/hole capture rate. Figure 3B also displays the effect of convoluting the calculated curves with a Gaussian function, so as to simulate the effect of the finite temporal resolution of the measurement system. The agreement of the measured and calculated curves, for which there are no fitting parameters, demonstrates that the finite value of $g^{(2)}(0)$ derives mostly from the limited time resolution of the measurement system, whereas two-photon emission from the device contributes to $g^{(2)}(0) < 0.07$ at an injection current of 2 μA. This represents more than an order of magnitude reduction in multiphoton emission events as compared to a classical light source displaying Poissonian statistics.

We also measured the second-order correlation function of the biexciton electroluminescence line of the dot at a diode current of 6 μA [Fig. 3A (iv)]. We find that the electroluminescence of the X_2 transition also displays photon anti-bunching, as reported recently for optical injection experiments (*13*, *22*). After emission of a biexciton photon, the dot is occupied by a single exciton and must therefore capture another electron-hole pair before a second biexciton photon can be emitted. In this case, the zero delay dip is shallower, $g^{(2)}(0) = 0.75$, than for the single exciton. However, as demonstrated by the calculated curve in Fig. 3A (iv), this is largely because the recovery in $g^{(2)}(\tau)$ is faster for the biexciton, which has a shorter lifetime, than for the exciton, and thus is more difficult to resolve experimentally for the biexciton. These results show that at higher injection currents, the diode can generate pairs of photons, one at the exciton energy of the dot and the other at the biexciton.

The emission time of the single photons from the diode can be regulated through pulsing of the injection current. Pulsed electrical injection leads to pulsed emission from the dot, which is single-photon emission provided that the pulse width is much less than the exciton lifetime. We biased the diode with rectangular voltage pulses at a repetition rate of 80 MHz, superimposed on a dc bias of 1.50 V. This dc voltage is just below the "turn-on" of the diode and was chosen so as to result in relatively little electroluminescence. For pulse durations considerably less than the exciton lifetime, we observe that the shape of the time-resolved electroluminescence is independent of pulse width and is similar to that excited by the 1-ps-wide laser pulses.

The second-order correlation function recorded for the X line with a pulse height of 0.15 V and a width of 400 ps [Fig. 3C (i)] shows only a weak peak at zero time delay, indicating a strong suppression of the multiphoton emission pulses from the dot. This contrasts with the pair correlation recorded for the wetting layer electroluminescence [Fig. 3C (ii)], for which a second photon is just as likely to be found in the same emission pulse as the first, as in any other. The area of the zero delay peak of the dot correlation is about 11% of those at finite delays, again indicating an approximate order of magnitude decrease in multiphoton emission pulses as compared to a Poissonian source of the same average intensity. This rate of multiphoton emission

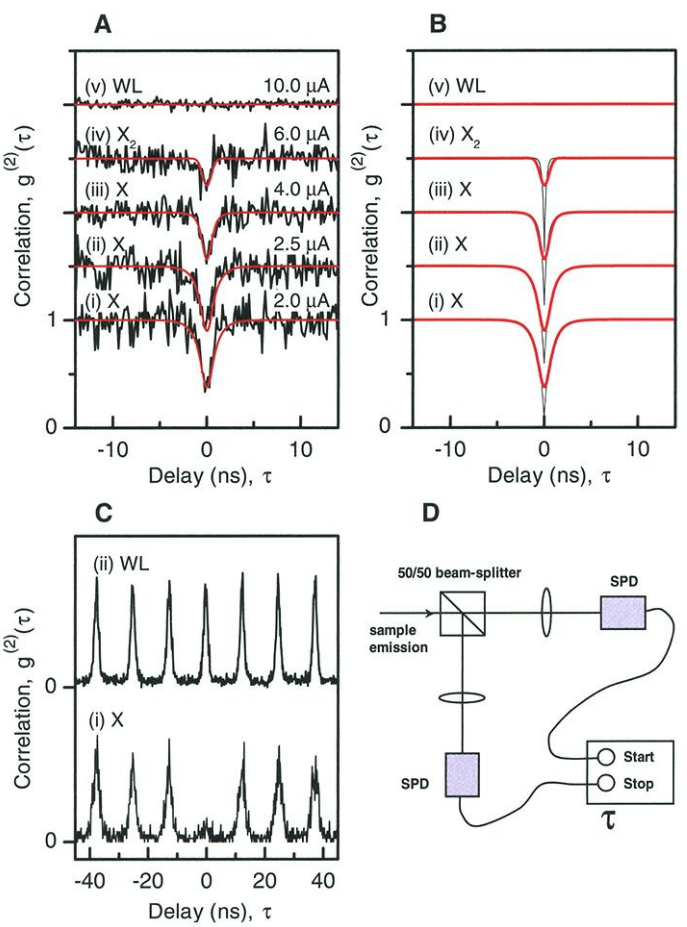

Fig. 3. Experimental proof of photon anti-bunching and single-photon emission in the electroluminescence of the device. (**A**) Second-order correlation function $g^{(2)}(\tau)$ of the electroluminescence of the single exciton line measured for different injection currents of (i) 2.0, (ii) 2.5, and (iii) 4.0 μA, as well as the biexciton line for 6 μA (iv). For comparison, the correlation trace of the wetting layer (WL) electroluminescence (v) is also shown. The curves are offset vertically for clarity. The solid lines are identical to the broadened calculated curves in (B). (**B**) Calculated second-order correlation function (thin black lines) for electron-hole pair injection rates of (i) 0.45, (ii) 0.55, (iii) 1.31, and (iv) 2.00 pairs per nanosecond and after convolution with a Gaussian function to mimic the finite temporal resolution of the measurement system (thick red lines). (v) Second-order correlation function of an emitter with Poissonian statistics. (**C**) Correlation measured for pulsed electrical injection for (i) quantum dot exciton and (ii) wetting layer emission. (**D**) Schematic of the experimental arrangement for correlation measurements.

could be further diminished by using shorter electrical pulses and reducing the background luminescence from the sample.

As for the prospects of realizing a single-photon–emitting diode for practical applications, the emission wavelength of the quantum dots chosen for study here is dictated by the spectral response of the Si single-photon detectors used in the experiments. However, InAs self-organized quantum dots can be tailored to emit at the wavelength used for long-distance fiber optic communications, around 1.3 μm (*24*). Furthermore, these longer wavelength quantum dots have much deeper carrier confinement potentials and thus emit efficiently at higher temperatures. In addition, the collection efficiency from the dot can be enhanced by means of an integrated cavity structure (*25*). Quantum dot light-emitting diodes may therefore provide an attractive source of either single photons or photon pairs for applications in quantum information technology and experiments in quantum optics.

References

1. G. Brassard, N. Lutkenhaus, T. Mor, B. C. Sanders, *Phys. Rev. Lett.* **85**, 1330 (2000).
2. E. Knill, R. Laflamme, G. J. Milburn, *Nature* **46**, 409 (2001).
3. For a review of early work, see D. F. Walls, G. J. Milburn, *Quantum Optics* (Springer, Berlin, 1994).
4. Th. Basche, W. E. Moerner, M. Orrit, H. Talon, *Phys. Rev. Lett.* **69**, 1516 (1992).
5. F. De Martini, G. Di Giuseppe, M. Marrocco, *Phys. Rev. Lett.* **76**, 900 (1996).
6. C. Brunel, B. Lounis, P. Tamarat, M. Orrit, *Phys. Rev. Lett.* **83**, 2722 (1999).
7. B. Lounis, W. E. Moerner, *Nature* **407**, 491 (2000).
8. L. Fluery, J.-M. Segura, G. Zumofen, B. Hecht, U. P. Wild, *Phys. Rev. Lett.* **84**, 1148 (2000).
9. P. Michler *et al.*, *Nature* **406**, 968 (2000).
10. P. Michler *et al.*, *Science* **290**, 2282 (2000).
11. C. Santori, M. Pelton, G. Solomon, Y. Dale, Y. Yamamoto, *Phys. Rev. Lett.* **86**, 1502 (2001).
12. V. Zwiller *et al.*, *Appl. Phys. Lett.* **78**, 2476 (2001).
13. R. M. Thompson *et al.*, *Phys. Rev. B* **64**, 201302R (2001).
14. C. Kurtsiefer, S. Mayer, P. Zarda, H. Weinfurter, *Phys. Rev. Lett.* **85**, 290 (2000).
15. R. Brouri, A. Beveratos, J.-P. Poizat, P. Grangier, *Opt. Lett.* **25**, 1294 (2000).
16. A. Imamoglu, Y. Yamamoto, *Phys. Rev. Lett.* **72**, 210 (1994).
17. J. Kim, O. Benson, H. Kan, Y. Yamamoto, *Nature* **397**, 500 (1999).
18. O. Benson, C. Santori, M. Pelton, Y. Yamamoto, *Phys. Rev. Lett.* **84**, 2513 (2000).
19. C. L. Foden, V. I. Talyanski, G. J. Milburn, M. L. Leadbeater, M. Pepper, *Phys. Rev. A* **62**, 011803R (2000).
20. D. Bimberg, M. Grundmann, N. N. Ledentsov, in *Quantum Dot Heterostructures* (Wiley, Chichester, UK, 1999).
21. Z. Yuan *et al.*, data not shown.
22. R. Hanbury-Brown, R. Q. Twiss, *Nature* **177**, 4497 (1956).
23. A. Kiraz *et al.*, preprint available at http://xxx.lanl.gov/abs/cond-mat/0108450.
24. R. Murray *et al.*, *Jpn. J. Appl. Phys.* **38**, 2022 (1999).
25. E. Moreau *et al.*, *Appl. Phys. Lett.* **79**, 6951 (2001).

3 October 2001; accepted 16 November 2001
Published online 13 December 2001;
10.1126/science.1066790
Include this information when citing this paper.

REPORTS

A One-Step Conversion of Benzene to Phenol with a Palladium Membrane

Shu-ichi Niwa,[1] Muthusamy Eswaramoorthy,[1] Jalajakumari Nair,[1] Anuj Raj,[1] Naotsugu Itoh,[1] Hiroshi Shoji,[2] Takemi Namba,[3] Fujio Mizukami[1]*

Existing phenol production processes tend to be energy-consuming and produce unwanted by-products. We report an efficient process using a shell-and-tube reactor, in which a gaseous mixture of benzene and oxygen is fed into a porous alumina tube coated with a palladium thin layer and hydrogen is fed into the shell. Hydrogen dissociated on the palladium layer surface permeates onto the back and reacts with oxygen to give active oxygen species, which attack benzene to produce phenol. This one-step process attained phenol formation selectivities of 80 to 97% at benzene conversions of 2 to 16% below 250°C (phenol yield: 1.5 kilograms per kilogram of catalyst per hour at 150°C).

Phenol is an important commodity chemical in industry: World production exceeded 6.6 megatons in 2000. Industrially, phenol has mainly been produced from benzene via cumene to cumene hydroperoxide (the so-called cumene process), but this three-step process (*1*) not only has a low phenol yield but is also highly energy-consuming. Furthermore, problems arise in treating its by-products, such as acetone and α-methylstyrene. Recently, direct oxidation of benzene to phenol by nitrous oxide (*2–4*) has been commercialized, but it is cost-effective only if nitrous oxide can be obtained cheaply as a by-product (*5*). Here we report an efficient one-step oxidation of benzene to phenol through direct hydroxylation of an aromatic ring in gas phase with oxygen activated by dissociated hydrogen obtained from a palladium membrane.

All direct hydroxylations (*6–16*) of aromatic nuclei with oxygen and hydrogen that have been reported so far have been done by simultaneously mixing an aromatic compound, oxygen, and hydrogen in liquid phase, using a very complicated system containing a multicomponent catalyst, a solvent, and some additives. Besides the possibility of an explosive gas reaction, these hydroxylations give only very low aromatic alcohol yields of 0.0014 to 0.69% (based on the amount of aromatic hydrocarbon initially used). We developed the direct hydroxylation of aromatic nuclei through a system in which hydrogen and oxygen are separately supplied or in which hydrogen is fed into a mixed gas stream of a substrate and oxygen through a metallic thin layer. This system is quite simple and appears to be practical when compared with other direct hydroxylations (*17–25*) reported recently.

The membranes were prepared by coating a porous α-alumina tube (NOK Corporation; α-Al_2O_3, 99.99%; outer diameter, 2.0 mm; inner diameter, 1.6 mm; void fraction, 0.43; average pore size, 0.15 μm) with a palladium thin layer (thickness, 1 μm; length, 100 mm) by means of a metallorganic chemical vapor deposition technique (*26*), using palladium(II) acetate (reagent grade) as the palladium source. At 300°C, the hydrogen and nitrogen permeation rates of the membranes prepared were 1.0 to 3.0 × 10^{-3} mol m^{-2} s^{-1} $Pa^{-0.5}$ and 0.1 to 1.0 × 10^{-10} mol m^{-2} s^{-1} Pa^{-1}, respectively.

A shell-and-tube reactor was set up with this membrane (Fig. 1) and used for the hydroxylation of aromatics. An aromatic hydrocarbon was fed into the membrane tube together with a mixed gas of oxygen and helium by bubbling it into the hydrocarbon liquid, and a pressurized mixture of hydrogen and helium (about 2 kg/cm^2) was flowed into the shell (outside of the tube). In some cases, the feeding of the gas mixtures was carried out in reverse; that is, hydrogen was fed inside of the tube and a hydrocarbon and oxygen were outside. The gaseous mixture coming out of the reactor was analyzed by an online gas chromatograph equipped with a capillary column (diameter, 0.25 mm; length, 25 m; packing reagent, PEG-20 M wide bore).

This palladium membrane reactor works well under mild conditions (below 250°C) for the direct hydroxylation of an aromatic nu-

[1]Institute for Materials and Chemical Process, National Institute of Advanced Industrial Science and Technology (AIST), Tsukuba Central 5, 1-1-1, Higashi, Tsukuba, Ibaraki 305–8565, Japan. [2]Research Center, Maruzen Petrochemical, 3 Goi, Minami-kaigan, Ichihara, Chiba 290–8503, Japan. [3]Tsukuba Technical Laboratory, NOK Corporation, 25 Wadai, Tsukuba, Ibaraki 300–4247, Japan.

*To whom correspondence should be addressed. E-mail: f-mizukami@aist.go.jp